The Astrophysical Journal, 744:167 (9pp), 2012 January 10 doi:10.1088/0004-637X/744/2/167

SOLAR RADIO TYPE-I NOISE STORM MODULATED BY CORONAL MASS EJECTIONS

K. Iwai[1], Y. Miyoshi[2], S. Masuda[2], M. Shimojo[3], D. Shiota[4], S. Inoue[5], F. Tsuchiya[1], A. Morioka[1], and H. Misawa[1]
[1] Planetary Plasma and Atmospheric Research Center, Tohoku University, Sendai, Miyagi 980-8578, Japan; kazumasa-iwai@pparc.gp.tohoku.ac.jp
[2] Solar-Terrestrial Environment Laboratory, Nagoya University, Nagoya, Aichi 464-8601, Japan
[3] Nobeyama Solar Radio Observatory, Nobeyama, Nagano 384-1305, Japan
[4] Advanced Science Institute, RIKEN (Institute of Physics and Chemical Research), Wako, Saitama 351-0198, Japan
[5] National Institute of Information and Communications Technology, Koganei, Tokyo 184-0015, Japan
Received 2011 May 2; accepted 2011 September 29; published 2011 December 22

ABSTRACT

The first coordinated observations of an active region using ground-based radio telescopes and the *Solar Terrestrial Relations Observatory* (*STEREO*) satellites from different heliocentric longitudes were performed to study solar radio type-I noise storms. A type-I noise storm was observed between 100 and 300 MHz during a period from 2010 February 6 to 7. During this period the two *STEREO* satellites were located approximately 65° (ahead) and −70° (behind) from the Sun–Earth line, which is well suited to observe the earthward propagating coronal mass ejections (CMEs). The radio flux of the type-I noise storm was enhanced after the preceding CME and began to decrease before the subsequent CME. This time variation of the type-I noise storm was directly related to the change of the particle acceleration processes around its source region. Potential-field source–surface extrapolation from the *Solar and Heliospheric Observatory*/Michelson Doppler Imager (*SOHO*/MDI) magnetograms suggested that there was a multipolar magnetic system around the active region from which the CMEs occurred around the magnetic neutral line of the system. From our observational results, we suggest that the type-I noise storm was activated at a side-lobe reconnection region that was formed after eruption of the preceding CME. This magnetic structure was deformed by a loop expansion that led to the subsequent CME, which then suppressed the radio burst emission.

Key words: Sun: corona – Sun: coronal mass ejections (CMEs) – Sun: magnetic topology – Sun: radio radiation

1. INTRODUCTION

Metric solar radio emissions indicate the existence of non-thermal electrons in the solar corona at altitudes of 0.1–1.0 solar radii (Rs). Type-I noise storms are one of the solar radio phenomena observed at a meter wavelength. The storms have two components; one is a discrete type-I burst of short duration with a narrow band, and the other is a noise storm continuum of long duration with a broad band. Both components show highly circular polarization, corresponding to the ordinary mode (Elgarøy 1977).

It is generally considered that non-thermal electrons that are trapped by closed magnetic field lines excite plasma waves. These excited plasma waves are converted into O-mode waves, which are finally observed as type-I noise storms. Although the process to produce non-thermal electrons is not well understood, some models have been proposed. For example, Benz & Wentzel (1981) suggested that a newly emerging magnetic field interacts with a pre-existing coronal magnetic field. The resulting magnetic reconnection would create non-thermal electrons. Spicer et al. (1982) suggested that electron acceleration takes place around a shock due to an emerging magnetic field.

Type-I noise storms are associated with active regions and sometimes with flares and coronal mass ejections (CMEs). Meanwhile, type-I noise storms often occur without flares, and typical durations are significantly longer than those of flares. Therefore, it is not necessarily the case that the existence of type-I noise storms is associated with solar flares. Benz et al. (2005) suggested that there is a weak correlation between X-ray flares and metric type-I noise storms. The onset or enhancement of type-I noise storms is related with sunspot evolution and flare-like coronal phenomena (Lantos et al. 1981; Raulin et al. 1991; Raulin & Klein 1994; Crosby et al. 1996; Malik & Mercier 1996; Bentley et al. 2000). Kerdraon et al. (1983) reported that the activity level of type-I noise storms increases after the brightening in white-light coronagraph images. Willson (2005) observed a transient increase in brightness and a gradual displacement of a 91 cm noise storm source using the Very Large Array (VLA) during the initial onset of a CME. The author suggested that the observed increase in brightness might be caused by the energy injected from the CME which increased the electron density or temperature in the middle corona. Kathiravan et al. (2007) provided a statistical study of type-I noise storms that commenced after CMEs. They observed 340 noise storms using the Nançay radioheliograph. The onsets of 196 noise storms out of 340 were observed within 13 hr from the CME liftoff time.

There are several reports suggesting that the activity level of type-I noise storms is also decreased by flares (Boehme & Krueger 1982; Aurass et al. 1990, 1993) and CMEs (Kahler et al. 1994; Chertok et al. 2001). Chertok et al. (2001) observed type-I noise storms using fixed-frequency observations of IZMIRAN and CMEs using the P78–1 SOLWIND coronagraph and SMM Coronagraph/Polarimeter. They observed decreases or nearly complete disappearances of type-I noise storms and suggested an association with CMEs, even though the CME front is located at a height of several solar radii.

From these previous studies, it appears that the activity of type-I noise storms is related to evolution of coronal magnetic structures and their ejecta. However, their effects on type-I noise storms are not well understood. This is because the properties of solar radio bursts depend on many processes such as particle acceleration, wave generation, and emission directivity that the flux of radio bursts can be modulated by any one of these (Li et al. 2008, 2009), and it is important to identify the plasma processes which cause a time variation of a type-I

noise storm. The best observation of a type-I noise storm is possible when a source region is located at the center of the solar disk because of the emission directivity (Caroubalos & Steinberg 1974), while a limb observation can easily capture the coronal loop structures and CMEs. Therefore, a special observational geometry is necessary to observe both type-I noise storms and CMEs simultaneously. This ideal observation has not been realized until the launch of the *Solar Terrestrial Relations Observatory* (*STEREO*).

In this study, we present the observation of a type-I storm from 2010 February 6 to 7 and investigate the relationship between the solar radio type-I noise storm and CMEs. Using ground-based radio telescopes, we observed a type-I noise storm whose source active region was located around the disk center. The visible coronagraph observations of the *STEREO* satellites which were located approximately 65° (ahead) and −70° (behind) from the Sun–Earth line enable us to trace the CMEs erupted from the disk center without any extrapolation. This is the first research for a type-I noise storm with its source region observed from a side view.

2. OBSERVATIONS

2.1. Ground-based Radio Observations

Iitate Planetary Radio Telescope (IPRT) is a ground-based radio telescope at the Iitate Observatory of Tohoku University in the Fukushima prefecture, Japan. IPRT was originally developed to observe Jovian radio emissions (Tsuchiya et al. 2010). The physical aperture of IPRT is 1023 m^2. The wide-band observation system was newly installed at IPRT for solar radio observations (Iwai et al. 2011). This system enables us to observe radio emissions in the frequency range between 100 MHz and 500 MHz. The minimum detectable sensitivity in this frequency range is smaller than 0.7 solar flux units (sfu) with a 10 ms time resolution and a 61 kHz frequency resolution. Simultaneous observations for both left-handed circularly polarized component (LCP) and right-handed circularly polarized component (RCP) are possible. The antenna tracked the Sun every 30 s from 0:00 UT (09:00 LT) to 5:00 UT (14:00 LT) during the observational period in this study.

Before and after the daily observational period of IPRT, we also used data from the U.S. Air Force Radio Solar Telescope Network (RSTN; Guidice et al. 1981) to detect radio bursts. The radio intensity at 245 MHz observed at Palehua, Hawaii and Learmonth, Australia was obtained from National Geophysical Data Center of NOAA.[6] Radio images at 150 MHz from Nançay Radioheliograph[7] (NRH: Kerdraon & Delouis 1997) are used to determine the location of the radio source region.

2.2. Spacecraft Observations

STEREO consists of two spacecraft which were located approximately 65° (ahead) and −70° (behind) from the Sun–Earth line during the observational period. We used COR1 and COR2 coronagraphs (Howard et al. 2008) from the Sun–Earth Connection Coronal and Heliospheric Investigation (SECCHI; Howard et al. 2002) to trace the propagation of CMEs from the outer corona to interplanetary space. The *Extreme Ultraviolet Imaging Telescope* (*EUVI*; Wuelser et al. 2004) is also used to detect coronal loop structures around the active region.

[6] http://www.ngdc.noaa.gov/stp/
[7] http://secchirh.obspm.fr/

3. RESULTS

Figure 1 shows the LCP and RCP radio dynamic spectra observed with IPRT in the top and bottom panels, respectively. Wide-band flux enhancements of type-III bursts were observed in both RCP and LCP during a period from 2:30 to 3:30 UT, indicating weak polarization of these type-III bursts. On the other hand, radio emissions which only have an RCP component appeared in the frequency range between 100 MHz and 300 MHz before the type-III bursts. These strongly polarized emissions are a so-called type-I noise storm. The flux of the type-I noise storm decreased from 1:00 to 2:00 UT and then disappeared after the type-III bursts. No type-I noise storm was observed for at least 3 hr after the disappearance.

Although the IPRT observation was performed only at the limited local time, the type-I noise storm had been observed continuously from February 6 to 7 by several radio observatories in the world. The type-III bursts were also observed several times during the observation period. The top panel of Figure 2 shows radio dynamic spectra between 100 kHz and 1 MHz observed by the WAVES spectrometer on board the *WIND* satellite (Bougeret et al. 1995) on February 6. Taking into consideration the frequency drift of type-III bursts, the type-III burst observed at 14:44 UT was expected to be emitted a few minutes before at a metric range. The bottom panel of Figure 2 shows a radio image at 432 MHz observed by Nançay Radioheliograph at 14:39 UT which is around the expected emission time of the Type-III burst (white contours) and at 14:45 UT (black contours) on February 6. Radio contours are plotted on the photospheric magnetogram observed by *SOHO*/MDI at 14:23 UT. There were two components of the radio source region at 14:39. One source region (named source 1) was located on the center of the active region. The other source region (named source 2) was located on the northwest of the active region. Source 2 was not observed at 14:45. As shown in the bottom panel of Figure 2, source 1 was observed continuously, while source 2 was observed intermittently several minutes before hectometric type-III bursts during the observation period of NRH. In addition, it is suggested that source 2 was located on the open field region from the potential field extrapolation, as will be shown in Figure 5. The source region of type-III bursts is expected to be located in the open field region (e.g., McLean & Labrum 1985), so that it is possible to consider that source 2 should be the source region of the observed type-III bursts and source 1 should be that of the observed type-I noise storm. The type-I source region was located on the center of the AR 11045 and its position was stable at least during the NRH observation period, which corresponds to the period before and after the IPRT observations.

Figure 3 shows the time profiles of the X-ray flux observed with GOES14 (panel (a)), radio flux at 246 MHz observed with RSTN Palehua and Learmonth Solar Observatories (panel (b)). Three M-class solar flares were observed around the active region AR 11045 during our observational period: Flare1, M2.9 started around 18:47 UT; Flare2, M1.3 started around 21:31 UT; and Flare3, M6.4 started around 02:20 UT. The start time, X-ray flux, and location of each flare are obtained from the GEMSIS-HINODE flare catalog as listed in Table 1.

The *STEREO* observations confirmed three CME eruptions (named CME 1, 2, and 3) associated with Flares 1, 2, and 3. Panel (c) of Figure 3 shows heights of the observed CME fronts from the solar surface derived from the *STEREO* observations. Three snapshots of coronagraph images during the three CME passages are presented in Figure 3. It has been believed that

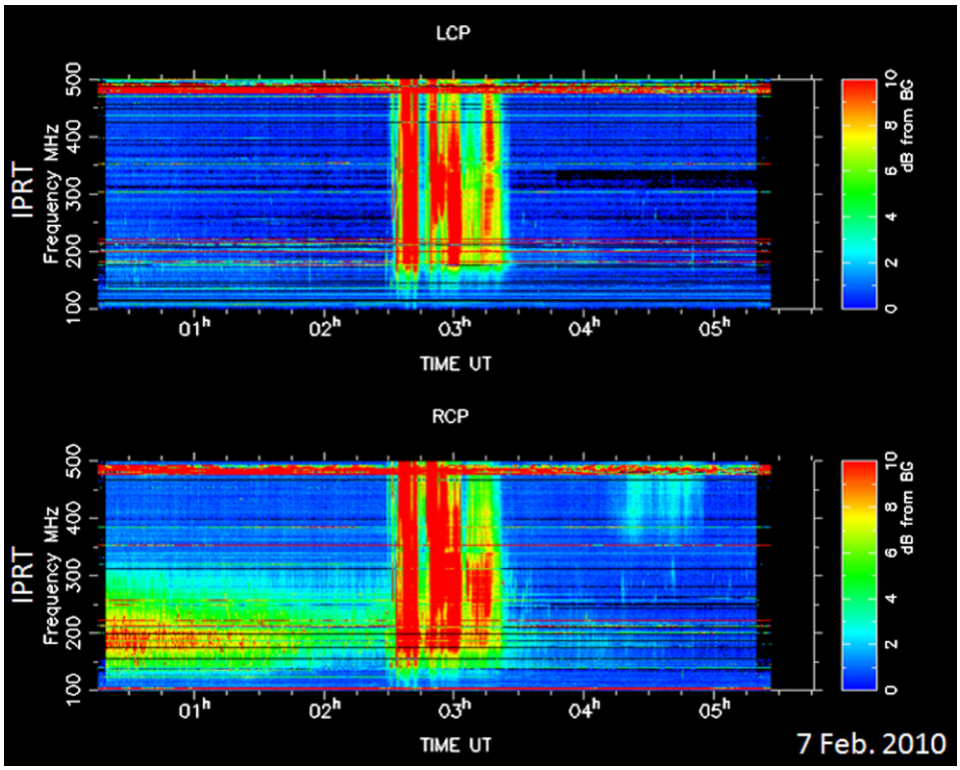

Figure 1. Radio dynamic spectra observed by IPRT on 2010 February 7; top: left-handed circularly polarized component and bottom: right-handed circularly polarized component.

Table 1
Characteristics of Observed Flares Obtained from the GEMSIS-HINODE Flare Catalog (http://st4a.stelab.nagoya-u.ac.jp/gemsis/hinode_flare/index.html)

No.	*GOES* Start	End	Peak	AR Location	X-ray Class
Flare 1	2010 Feb 6 18:47	2010 Feb 6 19:09	2010 Feb 6 18:59	N21E15	M2.9
Flare 2	2010 Feb 6 21:31	2010 Feb 6 21:42	2010 Feb 6 21:37	N22E12	M1.3
Flare 3	2010 Feb 7 02:20	2010 Feb 7 02:39	2010 Feb 7 02:34	N21E11	M6.4

type-I noise storms are emitted around the local plasma frequency (Elgarøy 1977), such that it is possible to estimate the altitude of the source region using the empirical coronal density model. The source region of radio emission between 100 MHz and 300 MHz is estimated to be between 0.1 and 0.5 Rs by assuming a 10 × Baumbach-Allen coronal density model (Allen 1947). This region is shown by a gray box in Figure 3(c). Although the real coronal density might be a different order of magnitude from the model, the altitude of the source region does not change significantly. (In fact for 100 MHz and 300 MHz, the source region is estimated to be between 0.05 and 0.3 Rs by assuming a 5 × Baumbach-Allen coronal density model.)

Type-III bursts were observed concurrently with Flares 1, 2, and 3. In addition to them, another type of radio emission which had a weaker intensity and a longer duration than the type-III bursts was observed twice between the flare events (from 20:00 UT to 21:30 UT and from 23:30 UT to 1:30 UT). The latter emissions correspond to the type-I noise storm shown in Figure 1. It is not clear whether the former radio emission also corresponds to a type-I noise storm because of the absence of spectrum and polarization measurements of IPRT. However, it is likely that these emissions measured at 246 MHz are associated with a type-I noise storm due to the similar characteristics of a longer duration and weaker intensity than type-III bursts.

There were two type-I noise storms within the interval of this study, and they were observed between the eruption of CME 1–2 and CME 2–3. In other words, the radio flux of type-I noise storm was enhanced after the eruption of CMEs 1 and 2. Then, it began to decrease before the eruption of the subsequent CMEs 2 and 3. For example, the flux of the noise storm was smaller than 20 sfu until 18:47, and then began to increase around 19:50 after the eruption of CME 1. Their flux reached 25–30 sfu at 20:10 and it did not decrease until around 21:15 when the CME2 started. At the time of decreasing intensity, the pre-existing CMEs (i.e., CMEs 1 and 2) were already located several solar radii above the solar surface, which is well above the height of the type-I source region. In fact, the second type-I noise storm observed from 23:30 UT began to decrease before the eruption of CME 3, which occurred at 2:20 UT the following day. At the time when the second type-I noise storm began to decrease (1:30 UT), CME 2 had already been ejected to outside 3 Rs.

Figure 4 shows EUV images observed by SECCHI/*EUVI* on board *STEREO-B*. An EUV loop appeared during 1:00–1:15 (a white arrow in panel (b) of Figure 4), which was around the same time as the type-I noise storm was decreasing. A flare occurred near the expanded loop about 60 minutes after the loop brightening.

Figure 5 shows coronal potential magnetic fields extrapolated by using the potential-field source–surface code (Shiota et al. 2008) with a *SOHO*/MDI (Scherrer et al. 1995) synoptic magnetogram[8] as the surface boundary conditions. On February 5, the active region showed a simple bipolar structure

[8] http://soi.stanford.edu/magnetic/index5.html

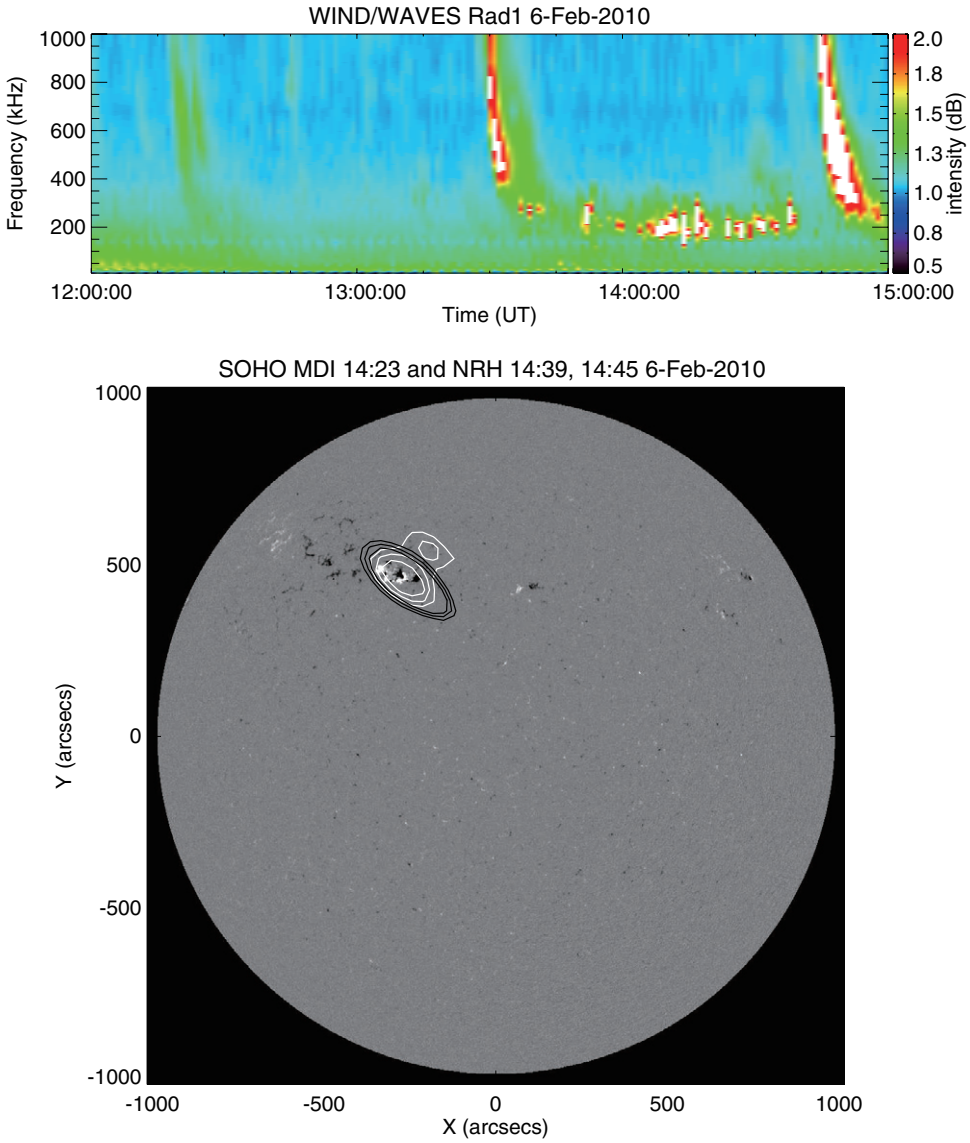

Figure 2. Top: radio dynamic spectra observed by *WIND*/WAVES Rad1 on 2010 February 6. Bottom: radio image at 432 MHz observed by Nançay Radioheliograph at 14:39 UT (white contours) and at 14:45 UT (black contours) plotted on the magnetogram observed by *SOHO*/MDI at 14:23 UT on 2010 February 6.

(left panel of Figure 5). On February 7, the observed active region formed a multipolar structure with the surrounding magnetic fields (regions A, B, C, and D in the right panel of Figure 5). The center of the active region AR11045 was located around central meridian (N24E01) at 23:30 UT on February 7. The observed flares and CMEs occurred around the center of the active region as shown in Table 1, which is the same as the boundary of regions B and C in Figure 3.

It should be noted that the coronal conditions changed after the eruption of CME 3. A fourth flare was observed around 5:00 UT but neither a CME nor a type-I noise storm was connected to this event (see Figures 1 and 3).

4. DISCUSSION

4.1. Summary of the Observations

Our observational results showed that type-I noise storms increased just after the CME eruption, which is consistent with previous studies (Kerdraon et al. 1983; Willson 2005; Kathiravan et al. 2007). The decrease of the type-I noise storms occurred when the front of the CME reached a height of several Rs. There were no CMEs at the heights of the type-I source region during the decreasing period. This point is also consistent with the previous work of Chertok et al. (2001). The *STEREO* multi-line-of-sight observations traced the eruption of the earthward propagating CMEs from the disk center and suggested that type-I noise storms decreased before the next CME eruption. The radio flux of type-I noise storm repeated an increasing and decreasing behavior twice. A coronal loop brightening was observed at the second decreasing phase of the type-I noise storm. The observed noise storm was emitted in the frequency range between 100 MHz and 300 MHz with a high degree of right-handed circular polarization.

The potential field extrapolations suggested that there was a multipolar magnetic system around the active region when the type-I noise storm was observed with the CMEs appearing around the center of the multipolar system.

4.2. A Model of Type-I Emission and Dissipation Process

From considering the observational results, we propose the following scenario to explain the time variation of the type-I

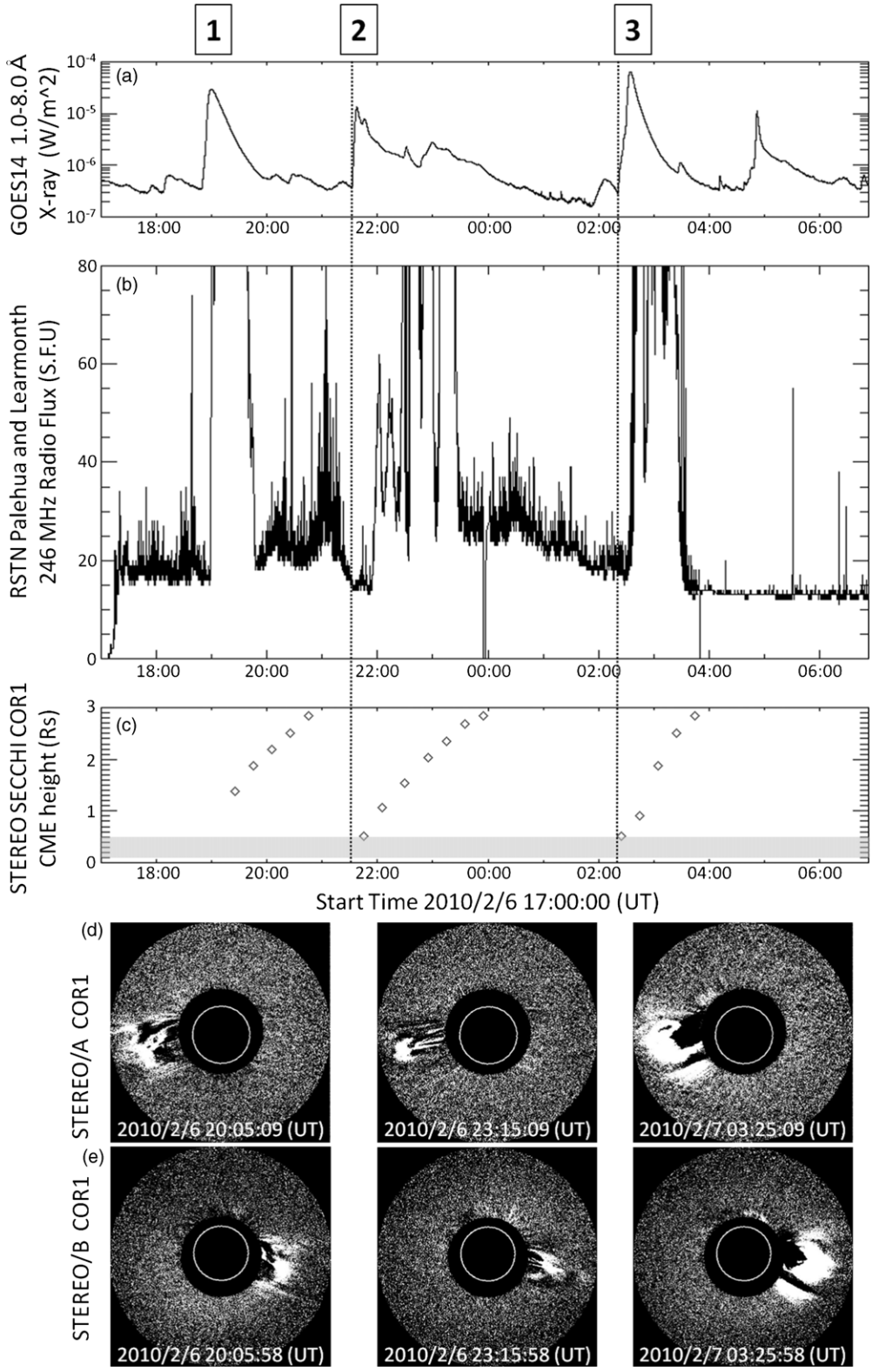

Figure 3. (a) Time profile of X-ray flux observed by GOSE14 on 2010 February 7 to 6. (b) Time profiles of metric solar radio flux around 246 MHz observed by the RSTN observatories. Observation data from Palehua observatory are plotted before 3:25 UT and after that data from Learmonth observatory are plotted. (c) Time profiles of the height of the leading edge of the CMEs observed by SECCHI/COR1 on board *STEREO*. Dotted lines indicate flare onset times. Panels (d) and (e): coronagraph difference images observed by SECCHI/COR1 on board *STEREO-A* and *B* at (left) 20:05, (center) 23:15 UT on 2010 February 6, and (right) 03:25 UT on 2010 February 7.

emissions. We assume that a CME occurred within a multipolar magnetic field region and is associated with a topology that is expressed by the "break out" model (Antiochos et al. 1999). Figure 6 shows schematics of the scenario for the type-I noise storm generation and dissipation proposed in this study. There are four phases in this scenario:

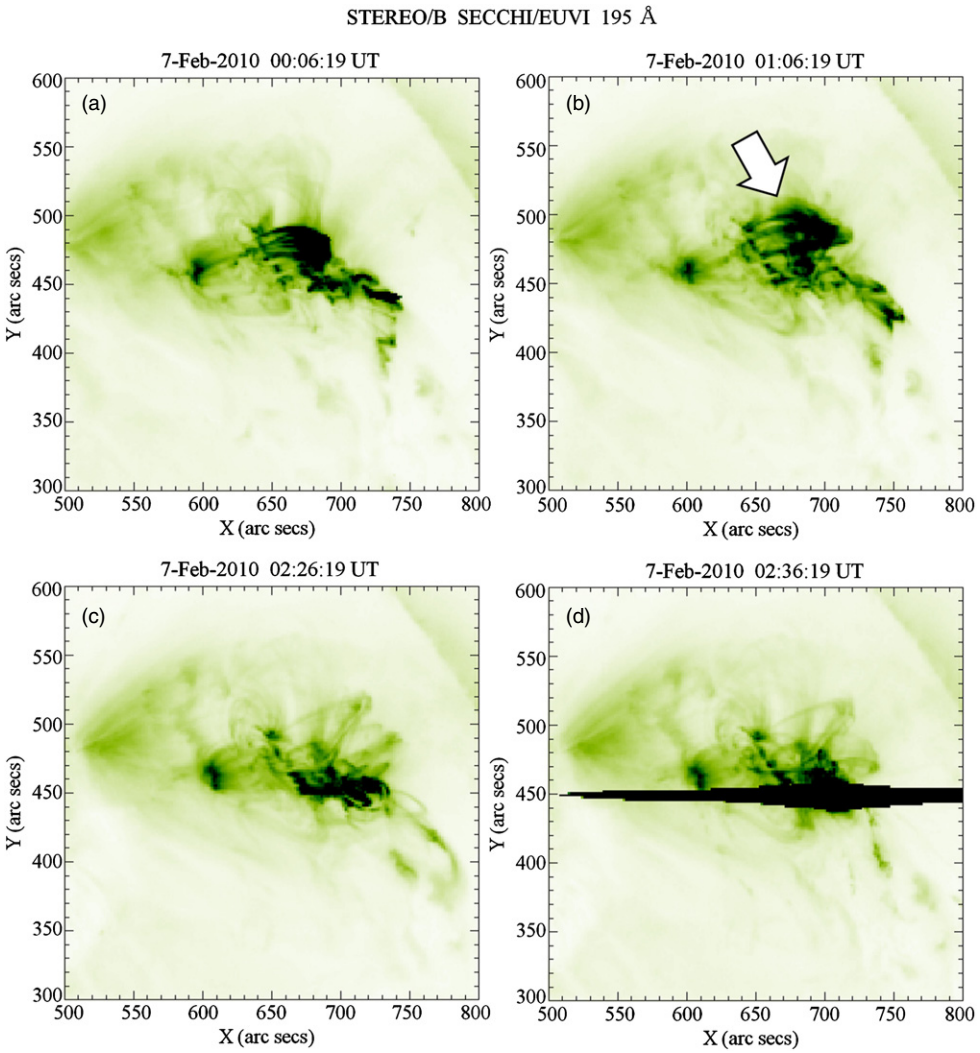

Figure 4. *STEREO-B* SECCHI/*EUVI* 195 Å images observed at (a) 00:06:19 UT when the radio noise storms were appearing, (b) 01:06:19 UT when the radio noise storms were decreasing, (c) 02:26:19 UT just before the flare, and (d) 02:27:04 UT just after the flare occurred on 2010 February 7. The coordinate system is determined by the position of *STEREO-B*. The heliographic longitude and latitude of *STEREO-B* were −70.518° and 1.371°, respectively. The white arrow in panel (b) indicates the brightening loop.

1. An active region forms a multipolar structure with the surrounding magnetic fields. There are loop structures connecting region A to B (loop AB), loop BC, loop CD, and loop AD. Then, the inner magnetic flux (loop BC) interacts with the external flux (loop AD) and expands to the upper corona. There are also open field lines near region C.
2. A flare and a CME occur in the multipolar system. Then type-III bursts are excited by the escaping high-energy electrons around the flare reconnection site (the red region of Phase-2).
3. After the eruption of the CME, the side-lobe fluxes (loops AB and CD) come together and reconnect at the flare current sheet (the red region of Phase-3). This side-lobe reconnection region is able to produce energetic particles which have free energy to generate type-I emissions. The gray region of Phase-3 locates the emission region for the type-I noise storm. It is expected that some non-thermal electrons leak from the open field lines located near the active region, and these leaked electrons emit type-III bursts.
4. The magnetic flux expansion of loop BC occurs again before the next CME eruption. This expansion causes deformation of the side-lobe reconnection region that is located above and suppresses the type-I noise storm emission. This phase corresponds to the first phase of the preceding CME.

After the eruption of the second CME, a side-lobe reconnection region is formed again and a type-I noise storm is also activated again. CMEs and coronal magnetic structures repeat, generating a type-I noise storm after the preceding CME and decreasing it before the subsequent CME in this model.

4.3 Comparison of the Model and Observational Results

As shown in Figure 6, we expect that there are four phases in the type-I noise storm model for the observations in this study. Each phase corresponds to the observational results. Phase-1 of our model requires a multipolar magnetic structure in the active region. The multipolar topology shown in the right panel of Figure 5 corresponds to Phase-1. In Phase-2, flares and CMEs occur along the magnetic neutral line of the multipolar magnetic structure. All the observed flares listed in Table 1 occurred around the center of the active region.

In Phase-3 of our model, a type-I noise storm is observed. From IPRT observations, we can derive the following parameters on radio emissions: time duration, frequency, and

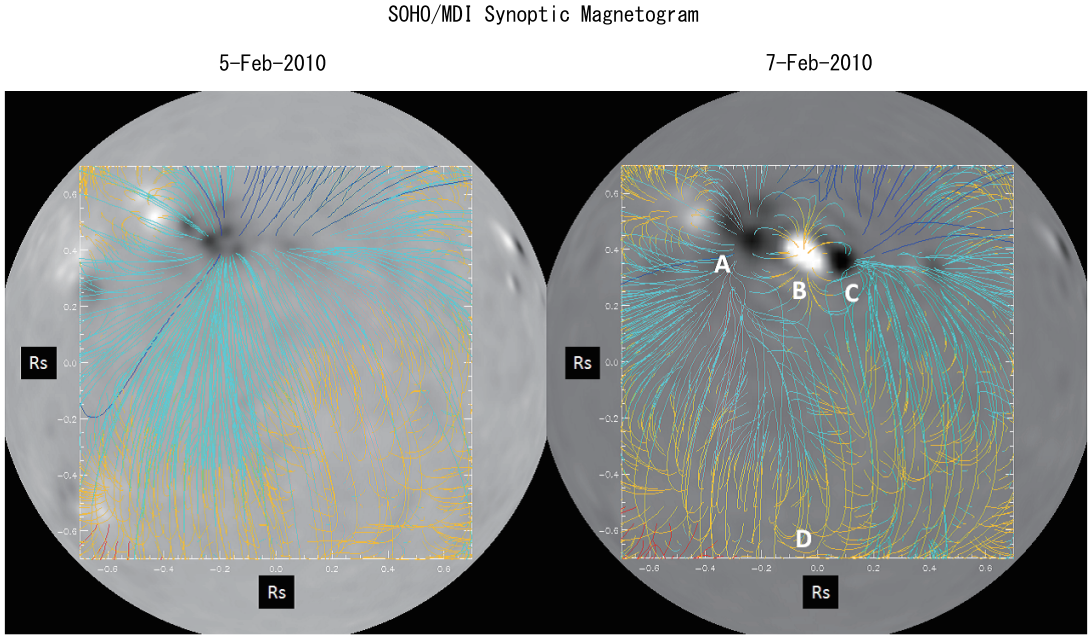

Figure 5. Coronal field lines obtained from potential-field source–surface extrapolations overlaid with the MDI synoptic magnetograms (left) on 2010 February 5 and (right) on 2010 February 7. The central Carrington longitudes of these pictures are 250°. Red and blue lines show open field lines with positive and negative magnetic polarities, respectively. Yellow and light blue lines show closed field lines with positive and negative magnetic polarities, respectively.

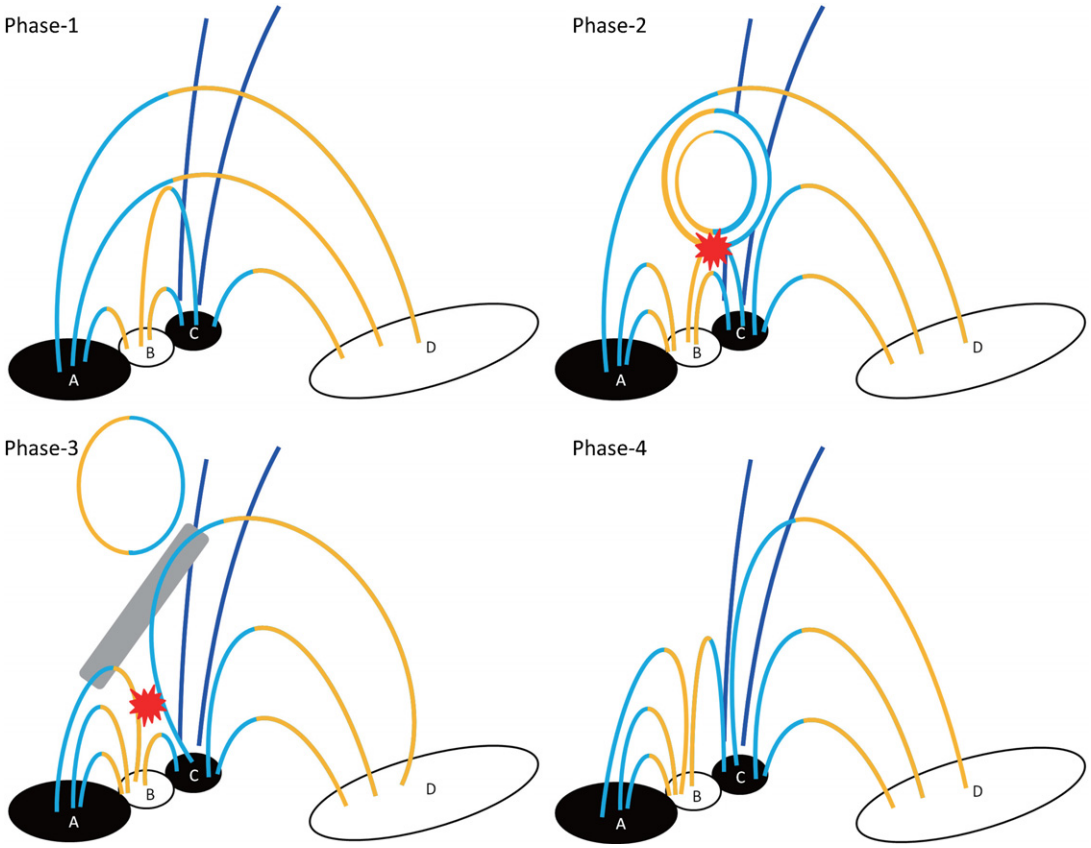

Figure 6. Schematics of the type-I noise storm region and ambient magnetic structures. White and black regions mean positive and negative magnetic polarity, respectively. Each region is labeled A–D corresponding to that indicated in Figure 5. Blue lines show open field lines with negative magnetic polarities. Yellow and light blue lines show closed field lines with positive and negative magnetic polarities, respectively. The gray region means the type-I noise storm region. The red regions mean the reconnection region.

polarization. Here, we discuss the observed variations of these parameters, considering the proposed model.

The observed type-I noise storms have relatively longer duration than other metric radio bursts such as type-III bursts (see Figures 1 and 3(b)). A current sheet or side-lobe region which is made after a break-out type CME (Phase-3 in Figure 6) is usually much less sheared and its reconnection proceeds slowly (Lynch et al. 2008). This side-lobe reconnection

region can supply weak but continuous energetic particles for a long time, which produces the successive type-I noise storm emissions.

The observed noise storm was emitted in the frequency range between 100 MHz and 300 MHz. The emission frequency remained within the same frequency band during the radio event (see Figure 1). This suggests that the radio source region was localized between the heights of 0.1 and 0.5 Rs. The decrease of the type-I noise storm occurred when the preceding CME front had reached a height of several solar radii (Figures 3(b) and (c)), which is significantly higher than the expected radio source altitude. Therefore, the preceding CME could not affect the source region. On the other hand, the magnetic structure which is made after the CME eruptions remained in the lower corona (Phase-3 in Figure 6).

The observed type-I noise storm had a high degree of right-handed circular polarization (see Figure 1). It is therefore suggested that the source region should be located along the leg of a magnetic loop anchored to negative magnetic polarity. In our model, particles are supplied to a closed magnetic loop with only negative magnetic polarity (gray region of Phase-3 in Figure 6), which is consistent with the observations of a highly right-handed polarized emission. As mentioned above, the modeled type-I noise storm which can be emitted in Phase-3 of Figure 6 is consistent with the intensity, frequency, and polarization characteristics of the observed type-I noise storms.

In a model of this study, an active region forms a multipolar structure with the surrounding large-scale fields. The polarization of the noise storm should be determined by the polarity of the leading sunspot and the footpoint region of the global magnetic field in the same hemisphere. This is consistent with previous observations (Le Squeren 1963; Payne-Scott & Little 1951). The polarity of the leading sunspot is the same as that of the footpoint region of the global magnetic field in the same hemisphere. Therefore, the configuration of our proposed model is consistent with the observational feature of the type-I polarization.

A magnetic structure in Phase-4 can be formed before the next CME eruption, while observed type-I noise storms decreased as shown in Figure 3. On the other hand, a coronal loop evolution was observed by *STEREO-B* (as shown in Figure 4) during the radio decreasing phase. EUV loop expansion or EUV brightening was sometimes observed with changes of type-I noise storm (Bentley et al. 2000; Willson 2005). The observed loop brightening might mean a deformation of ambient magnetic structures when the radio burst is decreasing.

Type-III bursts were also observed during the observation period (see Figure 2), suggesting the existence of open field lines near the flare region. The potential field extrapolations in Figure 5 suggest that there were open field lines located north of the C region. It is expected that these open field lines should be the trajectories of electron beams propagating to interplanetary space, and the escaping electrons excite the observed type III bursts.

4.4. Causes of the Noise Storm Generations and Depressions

The model of this study is based on an assumption that the observed time variations of a type-I noise storm are caused by variations of the particle acceleration processes at the source region. Besides the particle acceleration process, there are several possibilities which cause the time variations of radio burst intensity, such as directivity of the radio emission, radio propagation effects, and wave generation processes.

First, we consider the effect of directivity. A noise storm emission has relatively narrow directivity (Caroubalos & Steinberg 1974). Spatial deviation of noise storms may cause the change of the radio flux if the field line of the source region was deformed by a CME. However, for the cases presented in this paper, the active region was located almost on the center of the solar disk. Therefore, it is unlikely that the observer (Earth) is outside the directivity of the radio beam.

Next, we consider the propagation effect. A radio emission that has a lower frequency than the local plasma frequency cannot propagate through the medium. The observed type-I noise storms were emitted around 100–300 MHz. This means that the local plasma density of the radio source region was $\sim 10^9$ cm^{-3}. The typical plasma density in a CME at several Rs is much lower than $\sim 10^9$ cm^{-3} (Ciaravella et al 2003). Hence, it is not likely that the preceding CME could significantly affect the propagation of the type-I emissions to the observer.

Finally, we consider the wave generations. The efficiency of wave generations could also modulate radio emissions. Zaitsev et al. (1994) suggested that variation of the temperature, electron density, and magnetic field strength during a flare can change conditions of wave excitation and transformation of pre-existing type-I noise storms. However, the decreasing of radio bursts started before the flares in our case.

For the reasons mentioned above, we conclude that the change of the type-I noise storm emission observed in this study should be caused by particle acceleration processes at the source region.

5. CONCLUSION

We have investigated the relationship between the solar radio type-I noise storm and CMEs using ground-based radio telescopes and the *STEREO* satellites. The observed active region was located on the solar disk center. This location is well suited to observe type-I noise storms without any directivity effects. The two *STEREO* satellites were located around 65° (ahead) and −70° (behind) from the Sun–Earth line during this period. This location is well suited to observe earthward CMEs erupt from the center of the solar disk without any extrapolation. The radio flux of the observed type-I noise storm enhanced after the preceding CME and began to decrease before the subsequent CME. It is suggested that the observed time variation of the type-I noise storm is caused by variations of the particle acceleration processes at the source region. This is because other processes such as wave generation, propagation, and directivity hardly explain the observed time variation well. The potential-field source–surface extrapolation from *SOHO*/MDI magnetograms indicated that there was a multipolar magnetic system around the active region and CMEs occurred around the center of the multipolar system. Our observational results suggest that the observed type-I noise storm occurred at a side-lobe reconnection region that was formed after an eruption of the CME. This magnetic structure of the radio source region was deformed by a loop expansion that led to the next CME, which then suppressed the radio emissions. The observed EUV loop brightening at the second decreasing phase of type-I noise storm might be an observational counterpart at the lower corona.

We thank Neel Savani for valuable discussions. The SECCHI data are produced by an international consortium of Naval Research Laboratory, Lockheed Martin Solar and Astrophysics Lab and NASA Goddard Space Flight Center (USA), Rutherford Appleton Laboratory and University of Birmingham (UK), Max-Planck-Institut für Sonnensystemforschung

(Germany), Centre Spatiale de Liège (Belgium), Institut d'Optique Théorique et Appliquée, and Institut d'Astrophysique Spatiale (France). *SOHO* is a project of international cooperation between ESA and NASA. The Nançay Radio Observatory is funded by the French Ministry of Education, the CNRS, and the Région Centre. The Wind WAVES experiment is a collaboration of NASA/Goddard Space Flight Center, the Observatoire of Paris-Meudon, and the University of Minnesota. We thank NOAA National Geophysical Data Center for the RSTN radio data. This work was carried out by the joint research program of the Solar-Terrestrial Environment Laboratory, Nagoya University. K.I. was supported by Japan Society for the Promotion of Science (JSPS) Research Fellowships for Young Scientists.

REFERENCES

Allen, C. W. 1947, MNRAS, 107, 426
Antiochos, S. K., DeVore, C. R., & Klimchuk, J. A. 1999, ApJ, 510, 485
Aurass, H., Boehme, A., & Karlicky, M. 1990, Sol. Phys., 130, 19
Aurass, H., Hofmann, A., Magun, A., Soru-Escaut, I., & Zlobec, P. 1993, Sol. Phys., 145, 151
Bentley, R. D., Klein, K.-L., van Driel-Gesztelyi, L., et al. 2000, Sol. Phys., 193, 227
Benz, A. O., Monstein, C., & Meyer, H. 2005, Sol. Phys., 226, 121
Benz, A. O., & Wentzel, D. 1981, A&A, 94, 100
Boehme, A., & Krueger, A. 1982, Sol. Phys., 76, 63
Bougeret, J. L., Kaiser, M. L., Kellogg, P. J., et al. 1995, Space Sci. Rev., 71, 231
Caroubalos, C., & Steinberg, J. L. 1974, A&A, 32, 245
Chertok, I. M., Kahler, S., Aurass, H., & Gnezdilov, A. A. 2001, Sol. Phys., 202, 337
Ciaravella, A., Raymond, J. C., van Ballegooijen, A., Strachan, L., Vourlidas, A., Li, J., Chen, J., & Panasyuk, A. 2003, ApJ, 597, 1118
Crosby, N., Vilmer, N., Lund, N., Klein, K.-L., & Sunyaev, R. 1996, Sol. Phys., 167, 333
Elgarøy, Ø 1977, Solar Noise Storms (New York: Pergamon)
Guidice, D. A., Cliver, E. W., Barron, W. R., & Kahler, S. 1981, BAAS, 13, 553
Howard, R. A., Moses, J. D., Socker, D. G., Dere, K. P., & Cook, J. W. 2002, Adv. Space Res., 29, 2017
Howard, R. A., Moses, J. D., Vourlidas, A., et al. 2008, Space Sci. Rev., 136, 67
Iwai, K., Tsuchiya, F., Morioka, A., & Misawa, H. 2011, Sol. Phys., submitted
Kahler, S. W., Cliver, E. W., & Chertok, I. M. 1994, in IAU Colloq. 144, Solar Coronal Structures, ed. V. Rusin, P. Heinzel, & J.-C. Vial (Tatranska' Lomnica: VEDA), 271
Kathiravan, C., Ramesh, R., & Nataraj, H. S. 2007, ApJ, 656, L37
Kerdraon, A., & Delouis, J. M. 1997, in Coronal Physics from Radio and Space Observations, ed. G. Trottet (Berlin: Springer), 192
Kerdraon, A., Pick, M., Trottet, G., Sawyer, C., Illing, R., Wagner, W., & House, L. 1983, ApJ, 265, L21
Lantos, P., Kerdraon, A., Rapley, G. G., & Bentley, R. D. 1981, A&A, 101, 33
Le Squeren, A. M. 1963, Ann. Astrophys., 26, 97
Li, B., Cairns, I. H., & Robinson, P. A. 2008, J. Geophys. Res., 113, A06105
Li, B., Cairns, I. H., & Robinson, P. A. 2009, J. Geophys. Res., 114, A02104
Lynch, B. J., Antiochos, S. K., DeVore, C. R., Luhmann, J. G., & Zurbuchen, T. H. 2008, ApJ, 683, 1192
Malik, R. K., & Mercier, C. 1996, Sol. Phys., 165, 347
McLean, D. 1973, PASA, 2, 222
McLean, D. J., & Labrum, N. R. 1985, Solar Radiophysics (Cambridge: Cambridge Univ. Press)
Payne-Scott, R., & Little, A. G. 1951, Aust. J. Sci. Res. A, 4, 508
Raulin, J. P., Kerdraon, A., Klein, K.-L., et al. 1991, A&A, 251, 298
Raulin, J. P., & Klein, K.-L. 1994, A&A, 281, 536
Scherrer, P. H., Bogart, R. S., Bush, R. I., et al. 1995, Sol. Phys., 162, 129
Shiota, D., Kusano, K., Miyoshi, T., Nishikawa, N., & Shibata, K. 2008, J. Geophys. Res., 113, A03S05
Spicer, D. S., Benz, A. O., & Huba, J. D. 1982, A&A, 105, 221
Tsuchiya, F., Misawa, H., Imai, K., Morioka, A., & Kondo, T. 2010, Adv. Geosci., 19, 601
Willson, R. F. 2005, Sol. Phys., 227, 311
Wuelser, J.-P., et al. 2004, Proc. SPIE, 5171, 111
Zaitsev, V. V., Aurass, H., Kruger, A., & Mann, G. 1994, A&A, 291, 990